Towards Chloride-Free Organic Electrolytes for Rechargeable Aluminum Batteries

Zaher Slim [a] and Erik J. Menke *[a]

Broader context

Environmental implications brought about by global climate challenges and the ever-growing demands for renewable energy resources entail a quest for the development of large-scale, cost-effective and efficient energy storage systems. Successful design of rechargeable batteries based on multivalent ions (Mg^{2+}, Ca^{2+}, and Al^{3+}) can have far-reaching impacts on applications such as portable electronics, electric vehicles, and grid storage. As the most abundant metal in the Earth's crust, Al is an ideal candidate. Metallic Al anodes can, in theory, provide exceptionally high charge capacities. However, the lack of non-corrosive electrolytes has been a bottleneck in the advancement of a practical rechargeable battery. Shedding light on the electrodeposition of Al from chloride-free and chloride-rich organic electrolytes may pave the way for the development of next-generation Al-ion batteries. To that end, exploiting Al-based organic electrolytes for energy storage necessitates profound insights into the electrochemical and spectroscopic attributes of Al-ion complexes as will be conveyed by this study.

The corrosivity of chloride-based electrolytes is a major shortcoming in the practical realization of rechargeable aluminum batteries. Herein, the effect of Cl^- on Al speciation and electrochemistry in tetrahydrofuran was measured by employing theoretical and experimental approaches for three systems: $Al(OTF)_3/THF$, $Al(OTF)_3$ plus LiCl in THF, and $AlCl_3/THF$. The high consistency between measured and computed spectroscopic aspects associated with $Al(OTF)_3/THF$ electrolyte provided both a rationale for understanding Al complex-ion formation in a Cl^- free environment and an approach for examining the effect of Cl^- on Al speciation. Room-temperature Al plating was achieved from dilute solutions ([Al] = 0.1M) at potentials $\geq$ 0V (vs. Al/Al^{3+}). Cl^- is found to enable facile Al plating and SEM reveals that Al is electrochemically deposited as nanocrystalline grains.

The pursuit of high energy density for electrification of the transportation system and the demand for intermittent grid storage along with the significant uncertainty in material supplies for lithium-ion batteries[1,2] are propelling research efforts towards multivalent ion battery technologies, including those based on magnesium (Mg), calcium (Ca) and aluminum (Al).[3,4] Among post-lithium(Li) ion batteries, Al is of particular interest because of its superior theoretical volumetric capacity and low-cost compared to Li and other post- Li battery metals on account of its trivalency and high abundance.[5,6] However, making use of Al's remarkable capacity is challenging due to its relatively small ionic radius and high charge density, which inevitably leads to the formation of Al-ion complexes rather than "free" Al-ions in commonly employed chloroaluminate ionic liquids, diminishing the expected capacities of Al-ion batteries.[7] In spite of the recent advances in developing cathode materials,[8,9] and electrolytes,[6,10] the Al-ion battery remains in its infancy.[11] Accordingly, breaking new ground in Al-ion electrolyte chemistries for rechargeable Al batteries is of utmost significance.

Due to their ability to electrodeposit/strip Al , chloroaluminate ionic liquids based on aluminum trichloride ($AlCl_3$) are often investigated as electrolytes for Al-ion batteries.[12–28] Nevertheless, their integration into a practical Al-ion battery is hindered by severe drawbacks including the instability of cathode materials in these electrolytes leading to rapid capacity fading,[20] high corrosivity towards Al anodes[29] and stainless steel current collectors,[13] and side reactions that generate Cl_2 gas.[30,31]

Moreover, considering that molten salts are often limited to high operating temperatures,[6] organic solvents present an appealing choice for room temperature Al-ion battery application. The development of an organic electrolyte, however, is a challenging task that requires a fundamental understanding of the solute/solvent ion-dipole and coulombic interactions.[32]

[a] Chemistry & Biochemistry, University of California, Merced, Merced, California 95343, United States

†Electronic Supplementary Information (ESI) available: Full experimental section and additional data are provided. See DOI: 10.1039/x0xx00000x

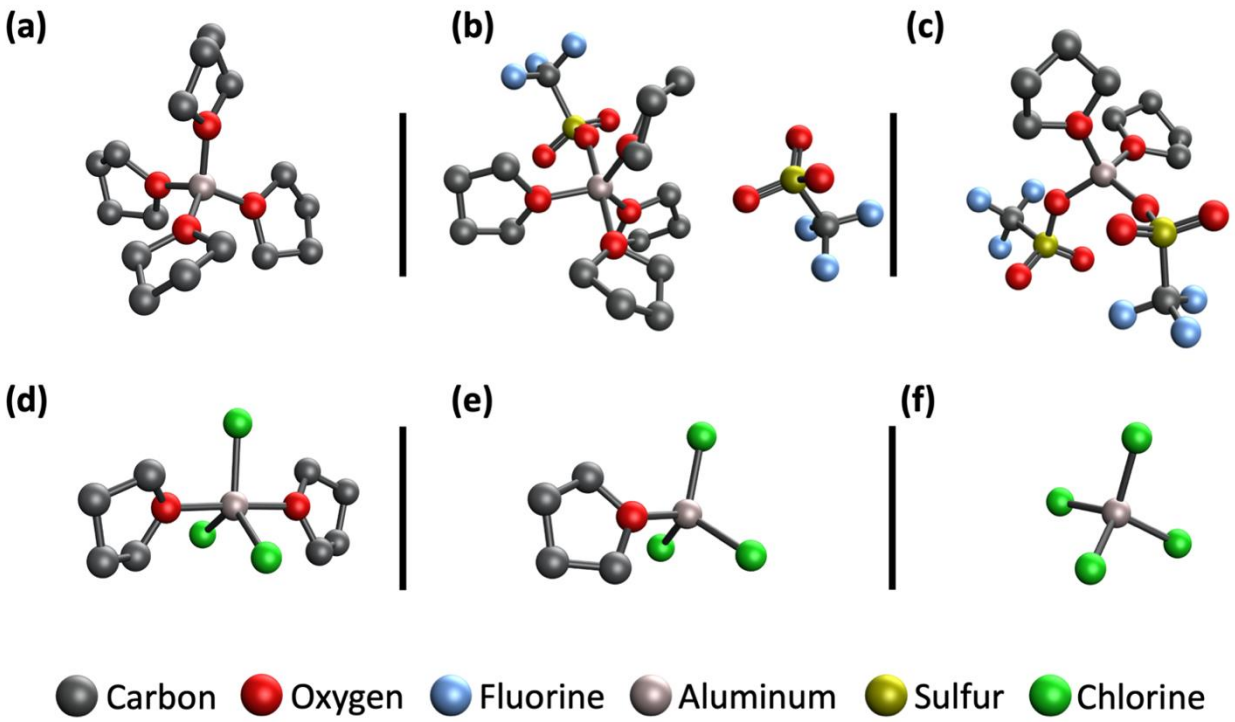

Fig. 1 Optimized structures (hydrogens not shown) of (a) $Al(THF)_4^{3+}$, (b) $[Al(THF)_4(OTF)][(OTF)]^+$, (c) $[Al(THF)_2(OTF)_2]^+$, (d) $AlCl_3(THF)_2$,(e) $AlCl_3(THF)$, and (f) $AlCl_4^-$.

Tremendous efforts have been dedicated to electrodeposit Al from a plethora of organic systems including $AlCl_3$ and lithium hydride(LiH) in diethyl ether,[33] $AlCl_3$ and lithium aluminum hydride ($LiAlH_4$) in tetrahydrofuran (THF) and benzene mixture,[34] $AlCl_3$ and $LiAlH_4$ in THF and toluene,[35] $AlCl_3$ and $LiAlH_4$ in THF,[36–39] aluminum tribromide($AlBr_3$) in aromatic hydrocarbons,[40,41] $AlBr_3$ in N,N-dimethylaniline,[42] $AlBr_3$ and potassium bromide (KBr) in ethylbenzene,[43] $AlCl_3$ in sulfones,[44–49] $AlCl_3$ in glycol ethers (glymes),[50–53] $AlCl_3$ in ethylene carbonate,[54] and $AlCl_3$ in gamma-butyrolactone (GBL).[55]

Unfortunately, these electrolytes are inherently corrosive and the prospects of practically implementing Al-ion batteries as electrochemical energy storage devices is contingent upon active chloride-free systems.[56] It is therefore imperative to investigate organic electrolytes based on alternative Al-salts. Inspired by the aforementioned challenges associated with Al-halides, researchers have sought to synthesize novel chloride-free Al-salts,[57–59] as well as explore the commercially available aluminum trifluoromethanesulfonate ($Al(OTF)_3$).[12,60–63] It is worth noting that employing $Al(OTF)_3$ as a potential Al-salt for Al-ion batteries has not been restricted to organic solvents, with its application in aqueous systems[64,65] and ionic liquids[66] having already been demonstrated. Despite these endeavours, the role free chlorides (Cl^-) play in Al-ion organic electrolyte chemistry, and a clear demonstration of Al electrodeposition using $Al(OTF)_3$, has not yet been established.

In our previous report,[63] we explored the ionic speciation and the electrochemical activity of Al-complexes in $Al(OTF)_3$/THF computationally and experimentally. Density functional theory (DFT) calculations coupled with Fourier transform infrared spectroscopy (FTIR) suggested that Al exists in these solutions as fully solvated Al-complexes, in addition to the presence of inner-sphere and outer-sphere trifluoromethansulfonate anions (OTF^-).[63] Further investigation at higher concentrations (>0.1M), presented herein, reveals that these solutions are dominated by $[Al(THF)_2(OTF)_2]^+$. The structure evolution of these species is depicted in Fig. 1a-c. In light of these findings and to ascertain the effect of Cl^- on the electrochemical behaviour of Al-ions, we report here evidence for the electrochemical reduction of Al-ions to Al-metal from THF through a comparative study that reveals the electrochemical behaviour and ionic speciation of Al-complexes in three electrolyte systems: $Al(OTF)_3$/THF, $Al(OTF)_3 + LiCl$/THF, and $AlCl_3$/THF.

In this work LiCl was chosen as an additive due to its ability to provide free Cl^- in THF, a result of the ionic character of the $Li - Cl$ bond in LiCl compared to the more covalent nature of the $Al - Cl$ bonds in $AlCl_3$. To examine the effect of Cl^- on Al speciation, a comprehensive investigation of computed versus measured vibrational frequencies was undertaken, with a summary of the DFT results is provided in the supporting material (Table S1). Our findings on the $AlCl_3$/THF solutions complement those of Derouault *et al.*,[67] where the major species in these solutions were found to be charge neutral $AlCl_3(THF)_2$ and $AlCl_3(THF)$ (shown in Fig. 1d and e). The spectral features of the $Al(OTF)_3$/THF and $AlCl_3$/THF solutions at various concentrations are then used to elucidate the reactions involving $Al(OTF)_3$ and LiCl in THF. Our results

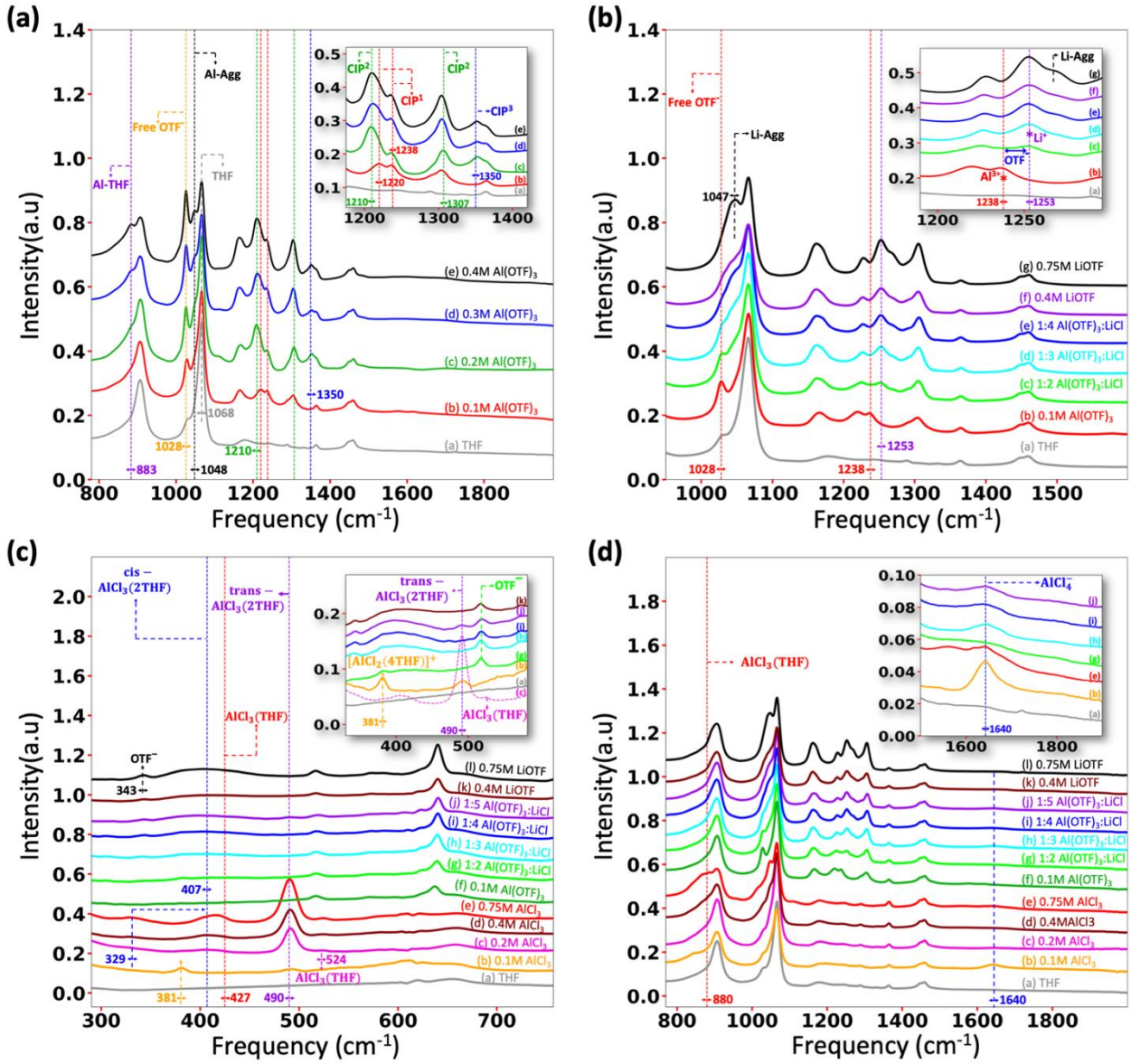

Fig. 2 FTIR spectra of various concentrations of Al and/or Li salts in THF. OTF^-: trifluoromethansulfonate anion, CIP: contact ion pair, Agg: aggregate, superscript 1: outer sphere OTF^-, superscript 2: inner sphere OTF^-, superscript 3: two inner sphere OTF^-.

suggest that this electrolyte is dominated by $AlCl_4^-$ (Fig. 1f) at $Al(OTF)_3$:LiCl mole ratios equal to or above 1:3, in addition to the ionic association between Li^+ and OTF^- in this electrolyte. The striking dissimilarities in the spectroscopic and electrochemical attributes for the Cl^- rich environments i.e. $AlCl_3/THF$ and $Al(OTF)_3 + LiCl/THF$, provide insight into the role of particular Cl^- containing Al-complexes in Al electrodeposition/stripping behaviour in THF.

A series of electrolyte solutions were prepared by dissolving appropriate amounts of Al-salt ($Al(OTF)_3$, $AlCl_3$) and/or Li-salt (LiOTF,LiCl) in THF. (See Materials and Methods section in ESI) FTIR spectra were collected and are shown in Fig 2.

Initially, it was crucial to examine the spectral regions corresponding to the complex-ion formation in the $Al(OTF)_3$/THF electrolyte at various concentrations (Fig. 2a). Previously,[63] we demonstrated that the peak at 1028 cm^{-1} is associated with symmetric stretch ($\nu_s SO_3$) of free OTF^- and that the 1200-1400 cm^{-1} region of the spectra displays bands assigned to the antisymmetric stretch of the OTF^-anions ($\nu_{as} SO_3$) for two types of contact ion pairs, outer sphere and inner sphere OTF^-, referred to here as CIP^1 and CIP^2, respectively. Re-examining this region, we find that the broad peak centred at 1210 cm^{-1} is likely a combination of two spectral components, a peak at 1220 cm^{-1}, CIP^1, assigned to $\nu_{as} SO_3$, another, CIP^2, at 1210 cm^{-1} assigned to $\nu C-S$ coupled with ν_sSO3 of OTF^-(Table S1). Upon access of an additional OTF^- to the inner solvation sphere of the Al-cation, a new peak appears both computationally and experimentally at ~1350 cm^{-1}. We attribute this peak to a third type of contact ion pairs, CIP^3, represented by the following species; $[Al(THF)_2(OTF)_2]^{1+}$ and $[Al(THF)_3(OTF)_2]^{1+}$. Although the predicted reaction energies for both complexes are similar

(Table S2), entropic factors are not accounted for in these calculations. As a result, we attribute the peak at ~1350 cm^{-1} to the tetrahedral complex $[Al(THF)_2(OTF)_2]^{1+}$.

Moreover, comparing the $Al(OTF)_3$/THF spectra to that of pure solvent (THF), we find that the peak at 1068 cm^{-1} becomes broader as the concentration increases, suggesting that this band is not only associated with THF but also $Al-CIP$ and/or Al-aggregates. [63,68]

The peak emerging at 883 cm^{-1}, as supported by our DFT calculations, can be assigned to $\nu(Al-O)$ coupled with τCH_2 of $Al-THF$ bond. (See table S1. in ESI) Finally, the peak observed at 1048 cm^{-1} is more prominent at concentrations >0.3M which suggest that this peak may be associated with ionic aggregates of $Al(OTF)_3$.

Based on these results the following dissociation reactions for Al-triflate in THF can be proposed:

$$Al(OTF)_3 + 4THF \rightarrow Al(THF)_4^{3+} + 3OTF^- \quad (1)$$
$$Al(OTF)_3 + 4THF \rightarrow [Al(THF)_4(OTF)][OTF]^+ + OTF^- \quad (2)$$
$$Al(OTF)_3 + 2THF \rightarrow [Al(THF)_2(OTF)_2]^{1+} + OTF^- \quad (3)$$

With considerable knowledge of the $Al(OTF)_3$/THF spectroscopic features in hand, the reaction between $Al(OTF)_3$ and LiCl in THF can now be studied. The progress of this reaction is depicted in the inset of Fig. 2b (See also Fig. S1). As LiCl is introduced to a 0.1M $Al(OTF)_3$ solution at mole ratios equal to or above 1:2, a transfer of the OTF^- from Al- to Li-ions is evident. This is illustrated by the peak shift from 1238 to 1253 cm^{-1}, which, according to our DFT calculations, may be assigned to $Al-CIP$[1] and $Li-CIP$, respectively. At 1:3 mole ratios, this region of the spectrum is identical to that of a solution of 0.4M LiOTF in THF. Thus, one may infer that a double displacement reaction between $Al(OTF)_3$ and LiCl takes place at 1:3 mole ratio according to reaction 4. While Li cations have OTF^- in their vicinity, the formation of LiOTF ionic aggregates can be excluded from the 1:3 electrolyte due to the absence of the peak at 1047 cm^{-1}, which is typically attributed to LiOTF aggregates,[69] and the shoulder peak at 1269 cm^{-1}, observed only in the 0.75M LiOTF/THF solution.

After establishing that the 1:3 electrolytes are primarily comprised of $AlCl_3$ and LiOTF, inspecting ionic species previously reported for $AlCl_3$/THF solutions is crucial. Alves *et al*. investigated $AlCl_3$/THF solutions by Raman spectroscopy and deduced that these electrolytes were dominated by $AlCl_4^-$ in dilute systems whereas $AlCl_3(THF)_3$ are favored at higher concentrations.[70] On the other hand, Derouault *et al*. investigated Al-halide ($AlCl_3$ or $AlBr_3$) in THF by FTIR and NMR spectroscopy,[67] and the results were compared to the FTIR and Raman spectra of solid Al-halide complexes.[71] The latter concluded that dissolving $AlCl_3$ in THF produced mainly $AlCl_3(THF)$, cis- and trans- isomers of $AlCl_3(THF)_2$, and $AlCl_4^-$ and $[AlCl_2(THF)_4]^+$ which resulted from slight dissociation of $AlCl_3(THF)_2$ according to a proposed equilibria which is provided in the ESI.

We note that our FTIR spectra for $AlCl_3$/THF appear identical to those of Derouault *et al*.[67] The spectra comparison with the $AlCl_3 + LiCl$/THF solution is shown in Fig. 2(c and d).

The distinct broad-band centered around 490 cm^{-1}, observed for all measured concentrations of the $AlCl_3$/THF solutions, has been assigned to the $\nu(Al-Cl)$ of $AlCl_3(THF)_2$ and $AlCl_4^-$ at 490 cm^{-1} and 494 cm^{-1}, respectively.[67] Comparatively, our DFT calculations suggest a peak for the $\nu_{as}(Al-Cl)$ at 476 and 488 cm^{-1} for the trans-$AlCl_3(THF)_2$ and a peak for the triply degenerate $\nu_{as}(Al-Cl)$ stretch for $AlCl_4^-$ at 477 cm^{-1}. Surprisingly, these peaks are absent in the 1:3 and 1:4 electrolytes, yet a weak-intensity peak is observed at 490 cm^{-1} for the 1:5 electrolyte. These intriguing disparities suggest that the peak at 490 cm^{-1} is attributed to $AlCl_3(THF)_2$ rather than $AlCl_4^-$. The absence of a peak at 477 cm^{-1} associated with $AlCl_4^-$ is probably due to the strong perturbation of the tetrahedral symmetry of $AlCl_4^-$ caused by the presence of excess amounts of Li^+, a phenomenon which has previously been reported for $LiAlCl_4$ melts.[72]

Additionally, DFT calculations suggest that the most thermodynamically favored reaction is that of $AlCl_3$ and Cl^- to produce $AlCl_4^-$ (Table S3). To confirm the presence of $AlCl_4^-$ in these electrolytes, the 800-1800 cm^{-1} regions of the spectra shown in Fig. 2d were examined. A broad peak ~1640 cm^{-1} emerges at 1:3 mole ratios, this peak is also present in dilute (0.1M) and concentrated (0.75M) $AlCl_3$/THF solutions. A similar band has been reported for $AlCl_4^-$ analogs,[73] which supports assigning this peak to $AlCl_4^-$.

In accordance with these findings, we propose the following dissociation mechanisms for the reaction between $Al(OTF)_3$ and LiCl in THF at 1:3 mole ratio:

$$Al(OTF)_3 + 3LiCl + 2THF \rightarrow AlCl_3(THF)_2 + 3LiOTF \quad (4)$$
$$AlCl_3(THF)_2 + Cl^- \rightleftharpoons AlCl_4^- + 2THF \quad (5)$$

Only when the amount of LiCl added to a 0.1M $Al(OTF)_3$/THF solution exceeded a 1:4 molar ratio did a peak appear at 490 cm^{-1}, indicating that an equilibrium exists between $AlCl_3(THF)_2$ and $AlCl_4^-$ with the former being produced only when substantial amounts of $AlCl_4^-$ have formed. This observation can be supported by the fact that THF is a much weaker Lewis base than Cl^-.

Moreover, the weak-intensity peak observed at ~381 cm^{-1} in the 1:2 solutions, concealed by an overlapping broad-band from LiOTF at higher mole ratios, is probably associated with $[AlCl_2(THF)_4]^+$, previously reported ~360 cm^{-1}.[67] The broad peak at 407 cm^{-1} is attributed to $\nu(Al-O)$[67] as supported by our DFT calculations for $AlCl_3(THF)$ (Table S1). Other bands attributed to this complex according to our DFT calculations are the peak at ~524 cm^{-1} (Fig. 2c) associated with $\nu_{as}(Al-Cl)$, and the peak at 880 cm^{-1} (Fig. 2d) associated with $\nu(Al-O)$ coupled with $\tau(CH_2)$(Table S1).

Finally, the vibrational frequencies of polymeric $AlCl_4^-$, namely $Al_2Cl_7^-$ and $Al_3Cl_{10}^-$ were calculated using DFT. Our results indicate that both species would have bands in the 200-600

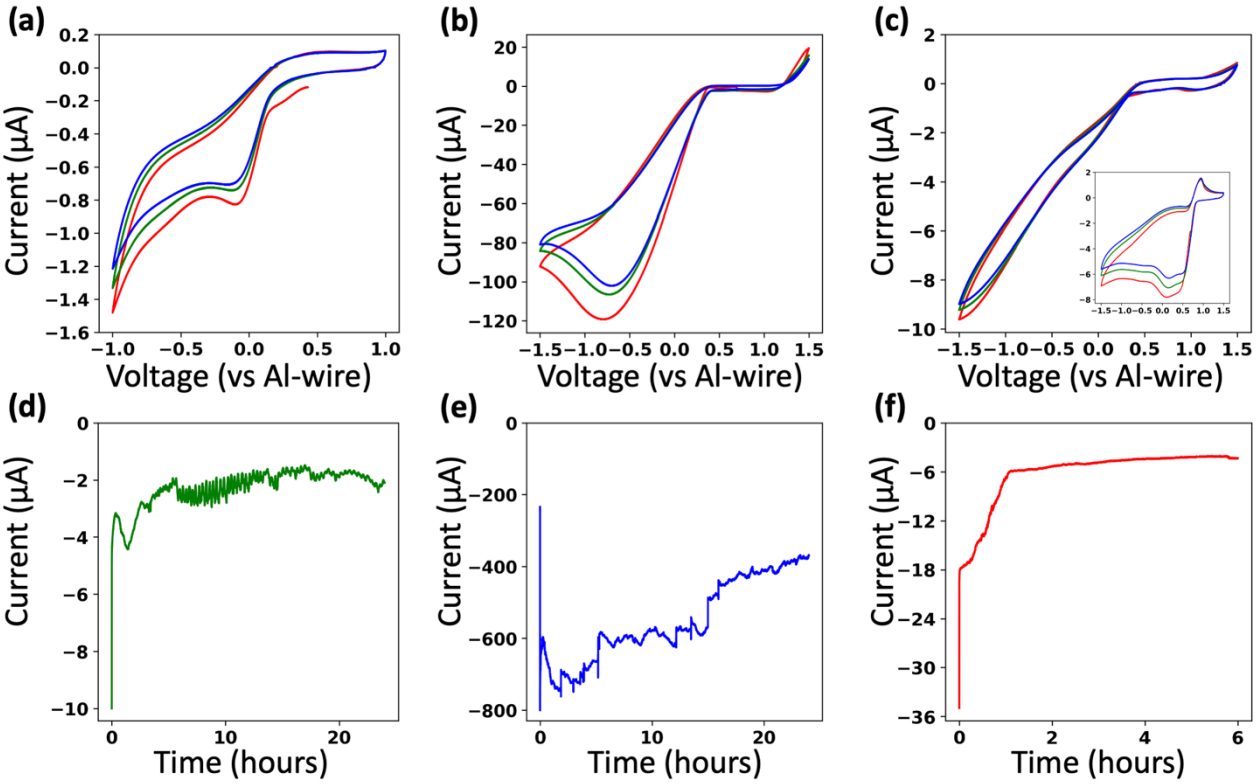

Fig. 3 Cyclic voltammograms on gold working electrode at 50 mV/s scan rate for (a) 0.1M $Al(OTF)_3/THF$, (b) 1:3 $Al(OTF)_3$: $LiCl/THF$ and (c) 0.1M $AlCl_3/THF$ with inset showing 0.75M $AlCl_3/THF$, and corresponding chronoamperograms on Cu-substrate of (d) 0.1M $Al(OTF)_3/THF$ at 0V, (e) 1:3 $Al(OTF)_3$: $LiCl/THF$ at +0.25V and (f) 0.1M $AlCl_3/THF$ at +0.25V (vs. Al/Al^{3+}).

cm^{-1} region. Although several peaks are observed at various concentrations in said region, it's highly unlikely that these peaks are attributable to polymeric $AlCl_4^-$. The only report of such species in similar systems, to our knowledge, is that of $AlCl_3/GBL$ solutions where the presence of $Al_3Cl_{10}^-$ was proposed at considerably high concentrations.[55] Thus, polymerization of $AlCl_4^-$ in THF, although possible, is unlikely to occur in dilute solutions (<1M), such as those studied here.

To evaluate the electrochemical behaviour of these electrolytes, cyclic voltammetry (CV) experiments were performed for 0.1M $Al(OTF)_3/THF$, 1:3 $Al(OTF)_3 + LiCl/THF$ and 0.1M $AlCl_3/THF$ using a gold working electrode in a standard three electrode setup, the results of which are shown in Fig. 3. The CV for 0.1M $Al(OTF)_3/THF$ electrolyte (Fig. 3a) reveals the electrochemical reduction of Al-ions with an onset reduction potential ca. +0.15V (vs. Al/Al^{3+}). The addition of LiCl at a 1:3 mole ratio (Fig. 3b) results in a shift in reduction potential to ca. +0.4V along with a dramatic increase in current, suggesting more facile Al electrodeposition in Cl^- rich environment, similar to shifts observed in the magnesium aluminum chloride complex electrolyte.[74] This electrolyte also exhibits a broad cathodic wave that extends beyond -1V, possibly due to co-deposition of Li which is expected around this potential versus the Al wire. CV measurements for the 1:2 mole solution were hindered by the formation of a gas bubble on the surface of the gold electrode, whereas the 1:4 and 1:5 solutions exhibited a similar CV profile to that of the 1:3 electrolyte (Fig. S3).

In contrast, the $AlCl_3/THF$ electrolyte exhibits a non-diffusion controlled electrochemical reduction ca. 0V for the 0.1M solution (Fig. 3c) while a drastic shift in reduction potential is evident at higher concentrations (0.75M) (inset of Fig. 3c). Two adjoint cathodic waves are observed ca. +0.25V, which we attribute to the electrochemical reduction of Al-ions. The shift in electrochemical activity as a function of increasing $AlCl_3/THF$ concentration is shown in Fig. S2. Additionally, an anodic peak is evident ca. +0.8V in the most concentrated $AlCl_3/THF$ solutions, this oxidative feature may have arisen as a result of partial Al-stripping caused by the increased acidity of the solution, likely due to the formation of $AlCl_3(THF)$ as we have previously revealed by DFT/FTIR analyses.

To further understand the nature of the acidic environment causing these immense differences in electrochemical behavior of Al-ions in the Cl^- rich environments (1:3 and 0.75M $AlCl_3/THF$), a clear description of the ionic profile of both electrolytes is necessary. According to previously discussed spectroscopy analyses, the electrochemically active Al species in the 1:3 electrolyte is likely the anionic species $AlCl_4^-$ arising from ligand transfer which is promoted by excess amounts of LiCl. In this system, $AlCl_4^-$ is associated with $Li - OTF$ CIP.

Comparatively, Al speciation in $AlCl_3/THF$ is much more diverse, and the origin of $AlCl_4^-$ is intricate. It is well known that $AlCl_3$ dimers may undergo symmetric and/or asymmetric cleavage when dissolved in ethereal organic solvents.[57,75] While DFT calculations revealed that both processes are equally plausibale in THF,[76] experimental evidence repeatedly

corroborates that these solutions are dominated by $AlCl_3(THF)_2$.[74,77] Interestingly, temperature dependant NMR spectroscopy for this system suggested that $AlCl_3(THF)_2$ undergoes self ionization to produce $[AlCl_4^-][AlCl_2^+(THF)_4]$.[67,78] Hence, the acidic character of the $AlCl_3/THF$ solution is perhaps also due to ionic association of the $AlCl_4^-$ to the highly acidic $[AlCl_2^+(THF)_4]$ rather than the charge neutral $Li-OTF$ CIP.

To gauge the likelihood of aluminum deposition, chronoamperometry was carried out on these three systems, in dilute solutions ([Al]=0.1M) using a Cu foil substrate in a standard three electrode setup. Chronoamperograms corresponding to Al-plating from 0.1M $Al(OTF)_3/THF$, 1:3 $Al(OTF)_3$: $LiCl/THF$ and 0.1M $AlCl_3/THF$ are shown in Fig. 3d, e and f, respectively. The potential for the $Al(OTF)_3/THF$ electrolyte was set to 0V vs. (Al/Al^{3+}), whereas the potential for the $AlCl_3/THF$ and 1:3 electrolyte was set to +0.25V (vs. Al/Al^{3+}). Over the course of these chronoamperometry experiment, a cathodic current was obtained for all three electrolytes. Despite the significantly lower electrodeposition potential of the 1:3 electrolyte, the measured current in this electrolyte is at least 2 orders of magnitudes higher than that of the $Al(OTF)_3/THF$ electrolyte. The total charge passed was calculated by integrating the chronoamperometry curves, and was found to be -196.3 mC, -47.47 C, and -131.8 mC for the Al-triflate/THF, 1:3 Al-triflate:LiCl/THF and AlCl3/THF, respectively. To confirm that the reductive processes observed in cyclic voltammetry and chronoamperometry plots correspond to electrochemical reduction of Al-ions to Al-metal, a scanning electron microscope (SEM) was used to evaluate the surface morphology of the Cu substrates. Fig. 4 shows a series of SEM images of an untreated Cu substrate (a,b), Al deposits obtained from $Al(OTF)_3/THF$ (c,d), 1:3 electrolyte (e,f), and $AlCl_3/THF$ (g-h).

Low magnification SEM images (Fig. S4) show that the 1:3 electrolyte exhibits high corrosivity as evident by the dark pits on the surface of the Al/Cu. High magnification SEM imaging for the Al deposits obtained from $Al(OTF)_3/THF$ reveal that these deposits undergo structural rearrangement during deposition to form streaks of nanoparticle agglomerates as shown in (Fig. S6) probably due to the non-homogenous surface of the Cu substrates.

To summarize, FTIR measurements complemented by DFT calculations provided unique insight into Al complex ion formation in Cl^- free ($Al(OTF)_3/THF$) and Cl^- rich ($AlCl_3/THF$ and $Al(OTF)_3 + LiCl/THF$) environments. The spectral features associated with the OTF^- anion were highlighted for the purpose of measuring the effect of Cl^- on Al-ion speciation and subsequently, the electrochemical behaviour of Al-ions. At the cost of high corrosivity, Cl^- significantly enhances the electrochemical activity of Al-ions. Spectral analyses coupled with CV measurements for the Cl^- rich systems suggest that a sufficiently acidic ionic environment may enable stripping of Al in THF. Finally, Al nanoparticles were deposited potentiostatically from dilute solutions ([Al]=0.1M) of all three systems.

Outlook

Organic electrolytes for Al-ion battery application are generally overlooked due to their volatility and high flammability. However, operational organic electrolytes typically comprise of concentrated electrolytes where the effect of free solvent is diminished leading to low volatility.[53] With regards to the flammability of these systems, this hurdle may be overcome by exploring additives that inhibit flammability via routes similar to those investigated for Li-ion[79] and Na-ion[80] electrolytes.

We speculate that Al can be electrochemically deposited from organic solvents of similar properties using $Al(OTF)_3$. Extending this work to other systems while exploring numerous additives may provide profound understanding of Al-anion and Al-solvent interactions which could potentially lead to an optimized, non-corrosive and safe organic electrolyte for practical Al-ion battery application.

Author Contributions

E.J.M: Conceptualization, Funding acquisition, Methodology, Project administration, Resources, Supervision, Validation, Writing – review & editing. Z.S: Data Curation, Formal analysis, Investigation, Software, Visualization, Writing – original draft.

Corresponding Author: Erik J. Menke
Email: emenke@ucmerced.edu

Acknowledgements

The authors acknowledge computing time on Multi-Environment Computer for Exploration and Discovery (MERCED) Cluster which is supported by National Science Foundation Grant no. ACI-1429783. Electron microscopy resources were provided by Imaging and Microscopy Facility (IMF) at UC Merced. Z.S thanks Kennedy Nguyen for helpful discussions on electron microscopy. Z.S is thankful to Hassan Harb for invaluable discussions on computational methodology.

Conflicts of interest

The authors declare no competing interests.

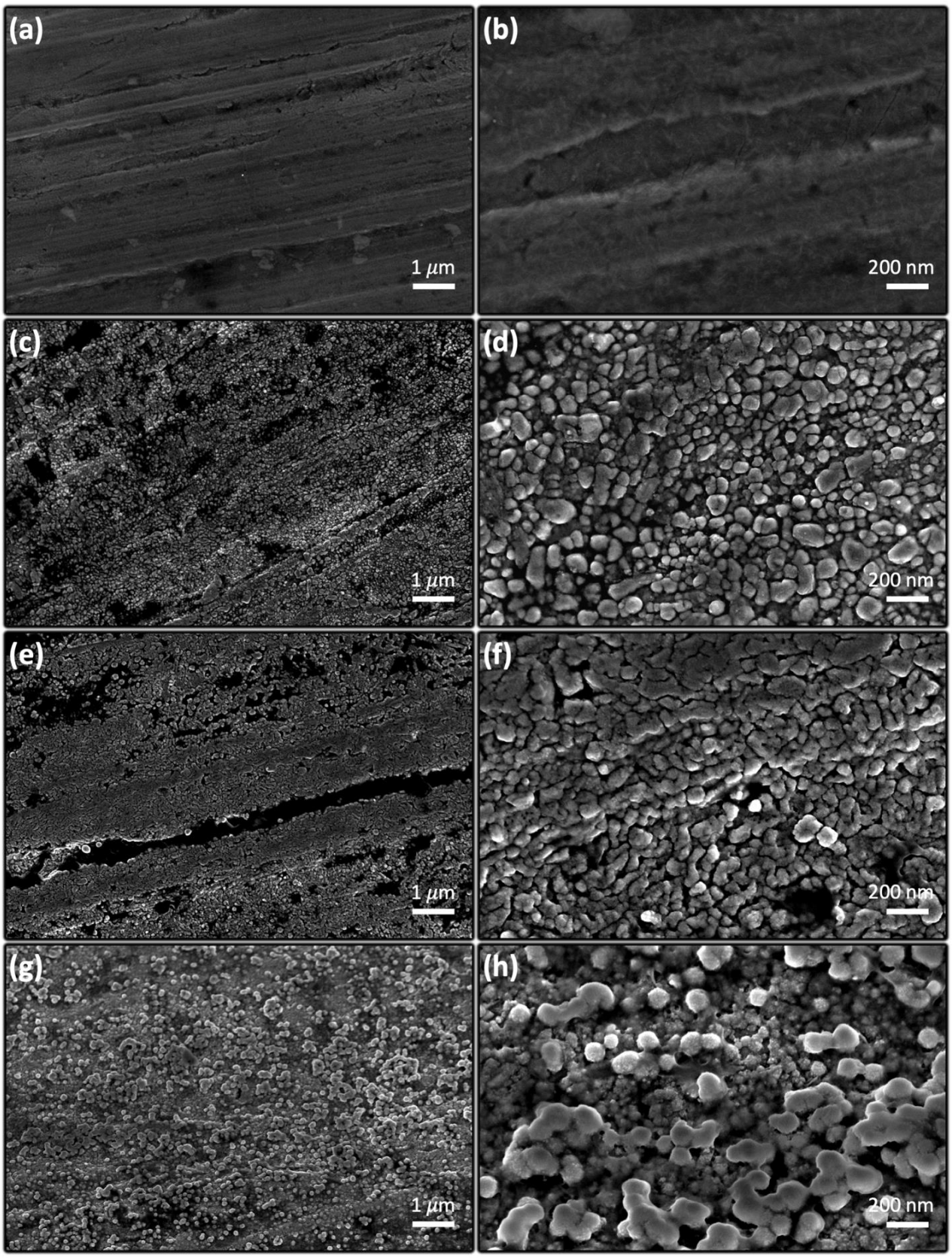

Fig. 4 SEM images of (a-b) untreated Cu substrate, Al electrodeposits on Cu-substrate (vs. $\mathrm{Al}/\mathrm{Al}^{3+}$) obtained from (c-d) 0.1M $\mathrm{Al(OTF)_3/THF}$ at 0V for 24 hours, (e-f) 1:3 $\mathrm{Al(OTF)_3{:}\,LiCl/THF}$ at +0.25V for 24 hours and (g-h) 0.1M $\mathrm{AlCl_3/THF}$ at +0.25V for 6 hours.

References

1 S. Jaffe, *Joule*, 2017, **1**, 225–228.
2 E. A. Olivetti, G. Ceder, G. G. Gaustad and X. Fu, *Joule*, 2017, **1**, 229–243.
3 Y. Liang, H. Dong, D. Aurbach and Y. Yao, *Nat. Energy*, 2020, **5**, 646–656.
4 M. Li, J. Lu, X. Ji, Y. Li, Y. Shao, Z. Chen, C. Zhong and K. Amine, *Nat. Rev. Mater.*, 2020, **5**, 276–294.
5 J. Muldoon, C. B. Bucur and T. Gregory, *Chem. Rev.*, 2014, **114**, 11683–11720.
6 J. Tu, W.-L. Song, H. Lei, Z. Yu, L.-L. Chen, M. Wang and S. Jiao, *Chem. Rev.*, 2021, **121**, 4903–4961.
7 E. Faegh, B. Ng, D. Hayman and W. E. Mustain, *Nat. Energy*, 2021, **6**, 21–29.
8 Z. A. Zafar, S. Imtiaz, R. Razaq, S. Ji, T. Huang, Z. Zhang, Y. Huang and J. A. Anderson, *J. Mater. Chem. A*, 2017, **5**, 5646–5660.
9 F. Wu, H. Yang, Y. Bai and C. Wu, *Adv. Mater.*, 2019, **31**, 1806510.
10 O. M. Leung, T. Schoetz, T. Prodromakis and C. P. de León, *J. Electrochem. Soc.*, 2021, **168**, 056509.
11 Y. Zhang, S. Liu, Y. Ji, J. Ma and H. Yu, *Adv. Mater.*, 2018, **30**, 1706310.
12 N. Jayaprakash, S. K. Das and L. A. Archer, *Chem. Commun.*, 2011, **47**, 12610–12612.
13 L. D. Reed and E. Menke, *J. Electrochem. Soc.*, 2013, **160**, A915.
14 L. Geng, G. Lv, X. Xing and J. Guo, *Chem. Mater.*, 2015, **27**, 4926–4929.
15 M.-C. Lin, M. Gong, B. Lu, Y. Wu, D.-Y. Wang, M. Guan, M. Angell, C. Chen, J. Yang and B.-J. Hwang, *Nature*, 2015, **520**, 324–328.
16 T. Gao, X. Li, X. Wang, J. Hu, F. Han, X. Fan, L. Suo, A. J. Pearse, S. B. Lee and G. W. Rubloff, *Angew. Chem., Int. Ed.*, 2016, **128**, 10052–10055.
17 N. P. Stadie, S. Wang, K. V. Kravchyk and M. V. Kovalenko, *ACS nano*, 2017, **11**, 1911–1919.
18 G. A. Elia, I. Hasa, G. Greco, T. Diemant, K. Marquardt, K. Hoeppner, R. J. Behm, A. Hoell, S. Passerini and R. Hahn, *J. Mater. Chem. A*, 2017, **5**, 9682–9690.
19 K. V. Kravchyk, S. Wang, L. Piveteau and M. V. Kovalenko, *Chem. Mater.*, 2017, **29**, 4484–4492.
20 H. Tian, S. Zhang, Z. Meng, W. He and W.-Q. Han, *ACS Energy Lett.*, 2017, **2**, 1170–1176.
21 M. Walter, K. V. Kravchyk, C. Böfer, R. Widmer and M. V. Kovalenko, *Adv. Mater.*, 2018, **30**, 1705644.
22 S. Wang, K. V. Kravchyk, A. N. Filippin, U. Müller, A. N. Tiwari, S. Buecheler, M. I. Bodnarchuk and M. V. Kovalenko, *Adv. Sci.*, 2018, **5**, 1700712.
23 D. Muñoz-Torrero, P. Leung, E. García-Quismondo, E. Ventosa, M. Anderson, J. Palma and R. Marcilla, *J. Power Sources*, 2018, **374**, 77–83.
24 H. Chen, H. Xu, S. Wang, T. Huang, J. Xi, S. Cai, F. Guo, Z. Xu, W. Gao and C. Gao, *Sci. Adv.*, 2017, **3**, eaao7233.
25 C. Yang, S. Wang, X. Zhang, Q. Zhang, W. Ma, S. Yu and G. Sun, *J. Phys. Chem. C*, 2019, **123**, 11522–11528.
26 D. J. Kim, D.-J. Yoo, M. T. Otley, A. Prokofjevs, C. Pezzato, M. Owczarek, S. J. Lee, J. W. Choi and J. F. Stoddart, *Nat. Energy*, 2019, **4**, 51–59.
27 Q. Zhou, D. Wang, Y. Lian, S. Hou, C. Ban, Z. Wang, J. Zhao and H. Zhang, *Electrochim. Acta*, 2020, **354**, 136677.
28 Q. Zhao, J. Zheng, Y. Deng and L. Archer, *J. Mater. Chem. A*, 2020, **8**, 23231–23238.
29 H. Wang, S. Gu, Y. Bai, S. Chen, N. Zhu, C. Wu and F. Wu, *J. Mater. Chem. A*, 2015, **3**, 22677–22686.
30 P. K. Lai and M. Skyllas-Kazacos, *J. Electroanal. Chem*, 1988, **248**, 431–440.
31 R. T. Carlin, W. Crawford and M. Bersch, *J. Electrochem. Soc.*, 1992, **139**, 2720.
32 H. Yang, H. Li, J. Li, Z. Sun, K. He, H.-M. Cheng and F. Li, *Angew. Chem., Int. Ed.*, 2019, **58**, 11978–11996.
33 D. E. Couch and A. Brenner, *J. Electrochem. Soc.*, 1952, **99**, 234.
34 N. Ishibashi and M. Yoshio, *Electrochim. Acta*, 1972, **17**, 1343–1352.
35 W. A. Badawy, B. A. Sabrah and N. H. Y. Hilal, *J. Appl. Electrochem.*, 1987, **17**, 357–369.
36 M. Yoshio and N. Ishibashi, *J. Appl. Electrochem.*, 1973, **3**, 321–325.
37 M. W. M. Graef, *J. Electrochem. Soc.*, 1985, **132**, 1038.
38 M. C. Lefebvre and B. E. Conway, *J. Electroanal. Chem.*, 2000, **480**, 34–45.
39 M. C. Lefebvre and B. E. Conway, *J. Electroanal. Chem.*, 2000, **480**, 46–58.
40 G. A. Capuano and W. G. Davenport, *J. Electrochem. Soc.*, 1971, **118**, 1688.
41 E. Peled and E. Gileadi, *J. Electrochem. Soc.*, 1976, **123**, 15.
42 T. Hisano, T. Terazawa, I. Takeuchi, S. Inohara and H. Ikeda, *Bull. Chem. Soc. Jpn.*, 1971, **44**, 599–603.
43 N. Yitzhack, P. Tereschuk, N. Sezin, D. Starosvetsky, A. Natan and Y. Ein-Eli, *J. Solid State Electrochem*, 2020, **24**, 2833–2846.
44 L. Legrand, A. Tranchant and R. Messina, *Electrochim. Acta*, 1994, **39**, 1427–1431.

45 L. Legrand, A. Tranchant and R. Messina, *J. Electrochem. Soc.*, 1994, **141**, 378.
46 L. Legrand, M. Heintz, A. Tranchant and R. Messina, *Electrochim. Acta*, 1995, **40**, 1711–1716.
47 L. Legrand, A. Tranchant and R. Messina, *Electrochim. Acta*, 1996, **41**, 2715–2720.
48 Y. Nakayama, Y. Senda, H. Kawasaki, N. Koshitani, S. Hosoi, Y. Kudo, H. Morioka and M. Nagamine, *Phys. Chem. Chem. Phys.*, 2015, **17**, 5758–5766.
49 M. Miyake, H. Fujii and T. Hirato, *Surf. Coat. Technol.*, 2015, **277**, 160–164.
50 A. Kitada, K. Nakamura, K. Fukami and K. Murase, *Electrochemistry*, 2014, **82**, 946–948.
51 A. Kitada, K. Nakamura, K. Fukami and K. Murase, *Electrochim. Acta*, 2016, **211**, 561–567.
52 A. KITADA, Y. KATO, K. FUKAMI and K. MURASE, *Journal of The Surface Finishing Society of Japan*, 2018, **69**, 310–311.
53 Z. Zhang, A. Kitada, S. Gao, K. Fukami, N. Tsuji, Z. Yao and K. Murase, *ACS Appl. Mater. Interfaces*, 2020, **12**, 43289–43298.
54 B. Zhang, Z. Shi, L. Shen, A. Liu, J. Xu and X. Hu, *J. Electrochem. Soc.*, 2018, **165**, D321.
55 X. Wen, Y. Liu, D. Xu, Y. Zhao, R. K. Lake and J. Guo, *J. Phys. Chem. Lett.*, 2020, **11**, 1589–1593.
56 J. Shi, J. Zhang and J. Guo, *ACS Energy Lett.*, 2019, **4**, 2124–2129.
57 T. Mandai and P. Johansson, *J. Phys. Chem. C*, 2016, **120**, 21285–21292.
58 M. Chiku, S. Matsumura, H. Takeda, E. Higuchi and H. Inoue, *J. Electrochem. Soc.*, 2017, **164**, A1841.
59 X. Wen, J. Zhang, H. Luo, J. Shi, C. Tsay, H. Jiang, Y.-H. Lin, M. A. Schroeder, K. Xu and J. Guo, *J. Phys. Chem. Lett.*, 2021, **12**, 5903–5908.
60 L. D. Reed, S. N. Ortiz, M. Xiong and E. J. Menke, *Chem. Commun.*, 2015, **51**, 14397–14400.
61 L. D. Reed, A. Arteaga and E. J. Menke, *J. Phys. Chem. B*, 2015, **119**, 12677–12681.
62 T. Mandai and P. Johansson, *J. Mater. Chem. A*, 2015, **3**, 12230–12239.
63 Z. Slim and E. J. Menke, *J. Phys. Chem. B*, 2020, **124**, 5002–5008.
64 C. Wu, S. Gu, Q. Zhang, Y. Bai, M. Li, Y. Yuan, H. Wang, X. Liu, Y. Yuan and N. Zhu, *Nat. Commun*, 2019, **10**, 1–10.
65 C. Yan, C. Lv, L. Wang, W. Cui, L. Zhang, K. N. Dinh, H. Tan, C. Wu, T. Wu and Y. Ren, *J. Am. Chem. Soc.*, 2020, **142**, 15295–15304.
66 H. Wang, S. Gu, Y. Bai, S. Chen, F. Wu and C. Wu, *ACS Appl. Mater. Interfaces*, 2016, **8**, 27444–27448.
67 J. Derouault, P. Granger and M. T. Forel, *Inorg. Chem.*, 1977, **16**, 3214–3218.
68 A. Bernson and J. Lindgren, *Solid State Ion.*, 1993, **60**, 31–36.
69 W. Huang, R. Frech and R. A. Wheeler, *J. Phys. Chem.*, 1994, **98**, 100–110.
70 C. C. Alves, T. B. Campos and W. A. Alves, *Spectrochim. Acta A*, 2012, **97**, 1085–1088.
71 J. Derouault and M. T. Forel, *Inorg. Chem.*, 1977, **16**, 3207–3213.
72 R. J. Gale and R. A. Osteryoung, *Inorg. Chem.*, 1980, **19**, 2240–2242.
73 R. Kore, S. P. Kelley, P. Aduri and R. D. Rogers, *Dalton Trans.*, 2018, **47**, 7795–7803.
74 K. A. See, Y.-M. Liu, Y. Ha, C. J. Barile and A. A. Gewirth, *ACS Appl. Mater. Interfaces*, 2017, **9**, 35729–35739.
75 A. H. Cowley, M. C. Cushner, R. E. Davis and P. E. Riley, *Inorg. Chem.*, 1981, **20**, 1179–1181.
76 J. B. Moss, MS Thesis, Utah State University, 2019.
77 M. C. Lefebvre and B. E. Conway, *J. Electroanal. Chem.*, 1998, **448**, 217–227.
78 H. Nöth, R. Rurländer and P. Wolfgardt, *Zeitschrift für Naturforschung B*, 1982, **37**, 29–37.
79 K. Deng, Q. Zeng, D. Wang, Z. Liu, G. Wang, Z. Qiu, Y. Zhang, M. Xiao and Y. Meng, *Energy Storage Mater.*, 2020, **32**, 425–447.
80 Y. Yu, H. Che, X. Yang, Y. Deng, L. Li and Z.-F. Ma, *Electrochem. Commun.*, 2020, **110**, 106635.